The Rising Star-Formation Histories of Distant Galaxies and Implications for Gas Accretion with Time

Casey Papovich[1,2]*, Steven L. Finkelstein[1,2], Henry C. Ferguson[3],
Jennifer M. Lotz[3,4]†, and Mauro Giavalisco[5]

[1] *Department of Physics and Astronomy, Texas A&M University, College Station, TX 77845-4242, USA*
[2] *George P. and Cynthia Woods Mitchell Institute for Fundamental Physics and Astronomy*
[3] *Space Telescope Science Institute, 3700 San Martin Drive, Baltimore, MD 21218, USA*
[4] *National Optical Astronomy Observatory, 950 N. Cherry Avenue, Tucson, AZ 85719, USA*
[5] *Department of Astronomy, University of Massachusetts, Amherst, MA 01003, USA*

ABSTRACT

Distant galaxies show correlations between their current star-formation rates (SFRs) and stellar masses, implying that their star-formation histories (SFHs) are highly similar. Moreover, observations show that the UV luminosities and stellar masses grow from z=8 to z=3, implying that the SFRs increase with time. We compare the cosmologically averaged evolution in galaxies at $3 < z < 8$ at constant comoving number density, $n = 2 \times 10^{-4}$ Mpc^{-3}. This allows us to study the evolution of stellar mass and star formation in the galaxy predecessors and descendants in ways not possible using galaxies selected at constant stellar mass or SFR, quantities that evolve strongly in time. We show that the cosmologically averaged SFRs of these galaxies increase smoothly from $z = 8$ to 3 as $\Psi(t) \sim t^{\alpha}$ with $\alpha = 1.7 \pm 0.2$. This conflicts with assumptions that the SFR is either constant or declines exponentially in time. Furthermore, we show that the stellar mass growth in these galaxies is consistent with this derived SFH. This provides evidence that the slope of the high-mass end of the IMF is approximately Salpeter unless the duty cycle of star formation is much less than unity. We argue that these relations follow from gas accretion (either through accretion or delivered by mergers) coupled with galaxy disk growth under the assumption that the SFR depends on the local gas surface density. This predicts that gas fractions decrease from $z = 8$ to 3 on average as $f_{\rm gas} \sim (1+z)^{0.9}$ for galaxies with this number density. The implied galaxy gas accretion rates at $z > 4$ are as fast and may even exceed the SFR: this is the "gas accretion epoch". At $z < 4$ the SFR overtakes the implied gas accretion rate, indicating a period where galaxies consume gas faster than it is acquired. At $z \lesssim 3$, galaxies with this number density depart from these relations implying that star formation and gas accretion are slowed at later times.

Key words: cosmology: observations – galaxies: evolution – galaxies: formation – galaxies: fundamental parameters – galaxies: high-redshift – galaxies: stellar content

1 INTRODUCTION

The process by which galaxies acquire their baryonic gas and convert it to stars is one of the main questions for theories of galaxy formation. However, it has been very difficult to constrain directly the evolution of these processes primarily because it is challenging to link the descendants and progenitors of galaxies at different snapshots in redshift. Currently, we have only a weak observational understanding of the star-formation histories (SFHs) of distant galaxies, which is arguably one of the most important quantities to measure because it governs directly how rapidly galaxies build up their stellar content.

Nevertheless, there are recent hints from the interpretation of observational data that distant galaxies experience SFHs where the SFR increases with time (decreasing redshift). The relatively tight correlation and low scatter between the star formation rates (SFRs) and stellar masses in distant galaxies (e.g., Daddi et al. 2007; Noeske et al. 2007; Stark et al. 2009; Magdis et al. 2010) imply that the majority of galaxies at high redshift sustain high levels of star for-

*E-mail: papovich@physics.tamu.edu
†Leo Goldberg Fellow

mation for prolonged time-scales of ~0.5–1 Gyr, with high "duty cycles".[1] Therefore short-lived starbursts driven by major mergers likely play a minor role. If the SFRs of these galaxies have been constant or declining in time, then it implies that the progenitors of these galaxies would have had higher specific SFRs (SFRs per unit stellar mass). However, Stark et al. (2009) observed a lack of evolution in the specific SFRs of UV-selected galaxies from $z = 4 - 6$, which excludes the possibility that galaxies at $z = 4$ have been forming stars at constant or declining rates since $z \gtrsim 5$. Finkelstein et al. (2010) noted that both the characteristic luminosity of the UV luminosity function, L^*_{UV}, and the stellar mass of galaxies at the characteristic luminosity increase with decreasing redshift from $z \sim 8$ to 3, which is most easily explainable if distant galaxies experienced SFRs that increase with time. Furthermore, recent work by Maraston et al. (2010) argue that rising SFHs better reproduce the observed colours of galaxies at $z \sim 2$ compared to models that decline with time (see also, Lee et al. 2010b).

Support for periods of extended star formation, such as that expected from a rising or constant SFH, also comes from kinematic measurements of many star-forming galaxies at $z \sim 1.5$–4, which show evidence for extended rotating gaseous disks not dominated by spheroids or mergers (e.g., Genzel et al. 2008; Daddi et al. 2009, 2010a; Förster-Schreiber et al. 2009; Law et al. 2009; Wright et al. 2009; Carilli et al. 2010; Tacconi et al. 2010). The existence of gaseous disks likely requires that distant galaxies form stars at a quasi-steady pace, and not in short periods of enhanced star formation such as merger-driven starbursts (see, Elmegreen et al. 2008; Bournaud et al. 2008; Dekel et al. 2009; Renzini 2009). Comparing galaxy SFRs to their gas masses yields gas consumption time-scales of a few hundred Myr, typically much shorter than a Hubble time at the observed redshift. In order for the galaxies to maintain their high levels of star formation, it follows that they must receive cold gas from the intergalactic medium (IGM) to replenish their supplies of fresh gas to fuel the continued star formation (e.g., Erb 2008; Prochaska & Wolfe 2009).

SFRs that increase with time for $z \gtrsim 3$ are an outcome from hydrodynamic and semi-analytic simulations. Maraston et al. (2010) favor SFRs that increase with time in part because these models reproduce the SFRs and stellar masses of galaxies from their semi-analytic model. Similar conclusions are obtained by Lee et al. (2010b) using SFHs from a semi-analytic model based on Somerville et al. (2001). Using a cosmological hydrodynamic simulation, Finlator et al. (2007) predict that galaxies at $z \geqslant 6$ experience SFRs that increase with time, and they show that these SFHs reproduce the UV luminosity functions and observed colours of distant galaxies (Finlator et al. 2006, 2007, 2010). Interestingly, the predicted SFHs in these simulations are scale-invariant, varying in mass only by a scale factor, implying that measurements of the SFHs of distant galaxies have strong constraining power on models. In the simulations, these smoothly-rising SFRs are driven by the net gas accretion (gas inflow minus gas outflow) regulated by

the competition between the growth of dark-matter haloes and decrease in cosmic density (e.g., Bouché et al. 2010; Dutton et al. 2010). Therefore, measuring the galaxy SFHs constrain both the growth of galaxy stellar mass, and the rate that gas accretion occurs.

Here, we use observations of galaxies to measure empirically their SFHs from $z = 8$ to 3. We compare galaxies at constant (comoving) number density over a range of redshift because this allows us to measure the evolution of the predecessors and descendants of galaxies in a relative meaningful way that is not possible using other selection methods. Our study is motivated in part by previous studies of galaxies at constant number density to infer evolution (see, e.g., Conroy & Wechsler 2009; van Dokkum et al. 2010). Studies of galaxy properties at fixed mass or luminosity compare galaxies of very different number density as a function of redshift, leading to potential biases (a variant of the well known *Malmquist bias*) when comparing galaxies selected at different redshifts. For example, Stark et al. (2009) study the evolution of galaxies at constant rest-frame UV *luminosity*, finding negligible evolution in the average stellar masses and ages of galaxies over the redshift range $4 < z < 6$. However, the number densities of galaxies at fixed luminosity change by factors >2 over this range (see figure 1 and discussion below) implying strong evolution. Comparing galaxy samples at constant number density has the benefit that it allows us to follow the evolution of the progenitors and descendants of galaxies across different redshifts (see Appendix A).

This paper is organized as follows. In § 2 we discuss the properties of galaxies at constant number density at redshifts $3 < z < 8$. In § 3 we constrain empirically the SFHs of galaxies at constant number density. In § 4 we compare the joint evolution of stellar mass and SFR for galaxies at constant number density, finding them to be largely consistent. In § 5 we use the SFR and stellar mass evolution combined with the expected growth of galaxy disks to predict the evolution of galaxy gas fractions at $3 < z < 8$. We provide discussion in support of using galaxy samples at constant number density in Appendix A, and we discuss how models with SFRs that increase with time affect the stellar masses of distant galaxies in Appendix B. Throughout this paper we use a cosmology with parameters, $H_0 = 70$ km s^{-1} Mpc^{-1}, $\Omega_{M,0}$=0.3, and Λ_0=0.7. All magnitudes quoted here are measured with respect to AB system, $m_{AB} = 31.4 - 2.5\log(f_\nu/1\,\mathrm{nJy})$ (Oke & Gunn 1983).

2 THE PROPERTIES OF GALAXIES AT CONSTANT NUMBER DENSITY

We compare galaxies at constant comoving number density, $n = 2 \times 10^{-4}$ Mpc^{-3}. For redshifts $3 < z < 8$ this corresponds approximately to the space density of $>L^*$ galaxies, and at $z \sim 0.1$ galaxies with this number density have stellar masses $>1.5 \times 10^{11}$ $M_\odot$, approximately twice that of the Milky Way Galaxy. Therefore, this number density corresponds to "typical" galaxies at these redshifts.

Comparing galaxies at constant number density has several advantages. In the absence of mergers the comoving number density of galaxies is invariant with time: galaxies will grow in baryonic mass through gas accretion and grow in stellar mass through star formation, but their number density will remain unchanged. In principle, identifying galaxies

---

[1] Here we take the *duty cycle* to be the ratio of the time duration of star-formation in galaxies relative to the total time interval probed by the galaxy survey, see, e.g., Lee et al. (2009).

at constant number density directly tracks the progenitors and descendants of the galaxies at different redshifts. Even a non-negligible number of mergers would have only a small effect on the progenitors and descendants of galaxies selected at constant number density (e.g., van Dokkum et al. 2010). In Appendix A we study how well selecting haloes at constant number density identifies their progenitors and descendants using simulated merger trees (Springel et al. 2005b). We found that selecting haloes at constant number density at different redshifts identifies 60–80% of the halo progenitors and descendants over the entire redshift range from $3.0 < z < 7.3$, and that this completeness fraction remains high even when selecting at constant number density based on SFR instead of halo mass. In contrast, studies of galaxies selected constant mass or luminosity correspond to highly heterogeneous samples at different redshifts for the reason that these quantities evolve strongly with time. Therefore, selecting galaxies at constant number density is a relatively straightforward means to study the properties of galaxy progenitors and descendants at different redshifts in a way that is unfeasible using other galaxy selections.

Here, we compare galaxies at constant number density based on their UV luminosity. Observations of galaxy clustering show that galaxy UV luminosity traces the halo mass tightly (e.g., Giavalisco & Dickinson 2001; Adelberger et al. 2005; Lee et al. 2006, 2009). Theoretically, the relation is unclear, and predictions span a wide range for the scatter between SFR (UV luminosity) and halo mass. While some models predict a tight relation, with scatter $\lesssim 0.1$ dex (e.g., Dutton et al. 2010; Finlator et al. 2010), others predict sizable scatter, ~ 0.3 dex (e.g., De Lucia et al. 2006; Bertone et al. 2007). To avoid an over-reliance on theoretical expectations, we make here the simple assumption that there is a one-to-one correspondence between the number density of galaxies at fixed halo mass and galaxies at fixed UV luminosity, which is supported by the observational evidence. However, in Appendix A we study how scatter in the relationship between UV luminosity and dark-matter halo mass impacts the completeness in the descendants and progenitors of galaxies selected at constant number density. To summarize, we find that increasing the scatter in this relation reduces the completeness in the number of halo descendants identified at lower redshift. However, even in models where the scatter is highest, the completeness is >40% over $3 < z < 7.3$, implying that the method tracks the descendants with high fidelity. Furthermore, the majority of the descendants of galaxies that are "missed" at lower redshifts have halo masses within 0.3 dex of the selected galaxies. We find some empirical evidence that galaxies have average SFHs that differ only by a scale factor related to total mass (§ 3), consistent with expectations from simulations Finlator et al. (2010). Therefore, the descendants that are missed likely have similar SFHs. Even though the descendants of galaxies at selected constant number density are incomplete, this method allows us to study the evolution of *averaged* galaxy populations over this redshift range.

2.1 Selecting Samples

Many studies have measured UV luminosity functions of galaxies from $z \sim 2$ to $z \gtrsim 8$ (e.g., Bouwens et al. 2004, 2006, 2010b,a; Reddy & Steidel 2009; Oesch et al. 2010b;
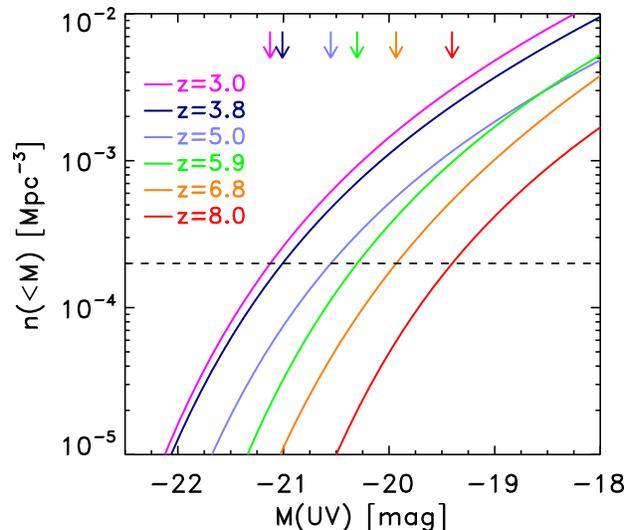

Figure 1. The comoving spatial number density of galaxies brighter than given absolute magnitude, $M_{\rm UV}$, derived by integrating the UV luminosity functions at $z = 3$ to $z = 8$ using values in table 1 from Reddy & Steidel (2009) at $z = 3.0$, Bouwens et al. (2007) at $z = 3.8$ to 5.9, and Bouwens et al. (2010a) at $z = 6.8$ and $z = 8.0$. We compared galaxies at constant number density by identifying at each redshift the absolute magnitude such that $n(<M'_{\rm UV}) = 2 \times 10^{-4}$ Mpc^{-3} denoted by the dashed horizontal line. The arrows indicate the value of $M'_{\rm UV}$ that corresponds to this number density for each luminosity function.

McLure et al. 2010). We integrated the UV luminosity functions to derive the number density of galaxies brighter than a given absolute magnitude at each redshift,

$$n(<M) = \int_{-\infty}^{M} \phi(M)\, \mathrm{d}M \qquad (1)$$

where $\phi(M)$ is the luminosity function in units of number Mpc^{-3} mag^{-1}. Figure 1 shows the integrated luminosity functions at each redshift. For the samples in this study we measured the evolving UV absolute magnitude, $M'_{\rm UV}(z)$, corresponding to the constant number density $n(<M'_{\rm UV}) = 2 \times 10^{-4}$ Mpc^{-3} at each redshift. These values are given in table 1 and indicated in figure 1.

The UV magnitude at constant number density $M'_{\rm UV}(z)$ brightens with decreasing redshift over this redshift range (similar to the evolution in $M^*_{\rm UV}$, see Bouwens et al. 2010c). The values of $M'_{\rm UV}(z)$ are based on the integral of the luminosity functions, and they are more robust than the individual luminosity function parameters. While there is non-negligible uncertainty on the parameters of the UV luminosity functions in the literature, this has little effect on the integral of the luminosity function. Using the $z = 8$ UV luminosity function from McLure et al. (2010) gives an absolute magnitude $M'_{\rm UV}(z)$ within 0.1 mag of the value in table 1.

Figure 1 illustrates an importance of using galaxy samples on the basis of constant number density rather than constant luminosity. Objects at constant luminosity (or stellar mass) correspond to very different number densities at different redshifts. The evolution in the UV luminosity functions corresponds to a change in number density of about a factor of 5 from $z = 7$ to $z = 3$ at fixed absolute magnitude,

Table 1. Properties of galaxies with comoving number density $n = 2 \times 10^{-4}$ Mpc^{-3}.

z [a]	M^* [b]	α [b]	ϕ^* [b]	ref.[c]	$A_{\rm UV}$ [d]	ref.[e]	$M'_{\rm UV}$ [f]	$\log \Psi$ [g]	$\log M_*$ [h]	ref.[i]	Original IMF[j]
				Derived from the UV luminosity functions							
2.3	-20.70	-1.73	2.8	RS09	1.71	B09	-21.06	1.64	9.9	R06,Sh05	Salpeter
3.1	-20.97	-1.73	1.7	RS09	1.77	B09	-21.1	1.69	10.0	R06,Sh05	Salpeter
3.8	-21.06	-1.76	1.1	B07	1.67	B09	-21.0	1.60	9.6	St09	Salpeter
5.0	-20.69	-1.69	0.90	B07	0.71	B09	-20.6	1.03	9.3	St09	Salpeter
5.9	-20.29	-1.77	1.2	B07	0.06	B09	-20.3	0.67	9.0	St09	Salpeter
6.8	-20.11	-1.94	0.90	B10	0.0	F10	-19.9	0.50	8.7	St09	Salpeter
8.0	-20.28	-2.00	0.38	B10	0.0	F10	-19.4	0.29	8.6	F10	Salpeter
				Derived from the Stellar mass functions							
0.1	10.96	-1.18	3.1	M09	...	...	...	...	11.2	...	Kroupa
1.5	10.91	-0.99	1.0	M09	...	...	...	...	11.0	...	Kroupa
2.5	10.96	-1.01	0.40	M09	...	...	...	...	10.7	...	Kroupa
3.5	11.38	-1.39	0.053	M09	...	...	...	...	10.3	...	Kroupa

[a] Median redshift of each sample.
[b] Characteristic magnitudes (masses) in units of magnitude (solar masses), faint end slope, and space density at the characteristic magnitude (mass) in units of 10^{-3} Mpc^{-3} mag^{-1} (10^{-3} Mpc^{-3} dex^{-1}).
[c] References for luminosity or mass function parameters: Reddy & Steidel (2009, RS09), Bouwens et al. (2007, B07), Bouwens et al. (2010a, B10), Marchesini et al. (2009, M09).
[d] Average attenuation at 1600 Å at $M'_{\rm UV}$ in magnitudes.
[e] References for the attenuation at 1600 Å: Bouwens et al. (2007, B07), Finkelstein et al. (2010, F10).
[f] Absolute magnitude of galaxies at comoving number density $n(<M'_{\rm UV}) = 2 \times 10^{-4}$ Mpc^{-3}.
[g] Extinction corrected SFR in units of $M_\odot$ yr^{-1} derived from $M'_{\rm UV}$ and A_{UV}.
[h] For UV-selected galaxies, these are the mean stellar mass in units of $M_\odot$ for galaxies with $M'_{\rm UV}$. For stellar-mass-selected galaxies, these are the stellar masses in units of $M_\odot$ for galaxies at comoving number density $n(>M'_*) = 2 \times 10^{-4}$ Mpc^{-3}.
[i] References for stellar masses for the UV-selected galaxies: Reddy et al. (2006, R06), Shapley et al. (2005, Sh05), Stark et al. (2009, St09), Finkelstein et al. (2010, F10). All stellar masses have been converted to a Chabrier IMF.
[j] Original IMF for stellar masses. Stellar masses using a Salpeter (1955) or Kroupa (2001) IMF were converted to a Chabrier IMF by multiplying by a factor of 0.54 and 1.13, respectively.

$M_{\rm UV} = -20$ mag. Galaxies selected at constant luminosity at different redshifts will result in samples with very different evolutionary paths compared to galaxies with constant number density (e.g., Conroy & Wechsler 2009).

2.2 Extinction and star formation rates

While the rest-frame UV light traces the instantaneous SFR of massive stars, it is subject to dust attenuation. Recent evidence shows that the mean dust attenuation decreases both with decreasing galaxy luminosity and increasing redshift (Reddy et al. 2008, 2010; Bouwens et al. 2009; Finkelstein et al. 2010). We quantify the amount of extinction for galaxies with $M'_{\rm UV}(z)$ using published values for the dust attenuation at rest-frame 1600 Å, $A_{\rm UV}$, for star-forming galaxies as a function of luminosity and redshift, listed in table 1. As there is little evidence for dust attenuation at $z \gtrsim 6$ (Bouwens et al. 2009, 2010c; Finkelstein et al. 2010) we assign $A_{\rm UV} = 0$ mag for these galaxies.

We combine the UV absolute magnitudes and dust attenuation to derive dust-corrected SFRs, $\Psi(z)$,

$$\Psi(z) = 10^{0.4[A_{UV} - 48.6 - M_{\rm UV}(z) - \mu(z)]}$$
$$\times 4\pi d_L(z)^2 \times 7.8 \times 10^{-29} \ M_\odot \ {\rm yr}^{-1}. \qquad (2)$$

where $\mu(z)$ is the distance modulus, and $d_L(z)$ is the lumi-

nosity distance in units of cm. The numerical factor is from Kennicutt (1998a) converted to a Chabrier (2003) IMF.[2]

There are several sources of uncertainty on the derived SFRs. The scatter in the dust extinction at $M'_{\rm UV}$ is non-negligible for galaxies at the lower end of our redshift range where the luminosity functions are well measured, producing uncertainties of a factor of order 2. There is little dust attenuation at the high end of our redshift range, but the luminosity function is less-well constrained, leading to uncertainties of a factor of order 2. One may expect these uncertainties to be lower when averaged over the galaxy population at each redshift. Lastly, the uncertainty in the UV luminosity–SFR calibration adds an additional 0.1 dex to the error budget (see footnote 2). Combining these, we apply a scatter of 0.3 dex to all SFR values for galaxies at $3 < z < 8$ in this study.

---

[2] Throughout we derive SFRs and stellar masses assuming the IMF of Chabrier (2003). The stellar mass and SFR of a stellar population with a Chabrier IMF are factors of 1.8 lower than for the IMF of Salpeter (1955), and factors of 1.13 higher than for IMF of Kroupa (2001). We note that calibration between the SFR and UV luminosity depends on the assumed SFH. We adopt the relation above, which assumes a constant SFH (Kennicutt 1998a). The SFR calibration for the UV luminosity for the SFH we derive below (equation 3) is within 30% for the stellar population ages considered here.

2.3 Stellar masses

Various studies have derived stellar masses, M_*, for high-redshift galaxies by modeling the rest-frame UV-to-near-IR data (e.g., Shapley et al. 2005; Papovich et al. 2005, 2006; Reddy et al. 2006; Stark et al. 2009; Finkelstein et al. 2010; Labbé et al. 2010a). We use these results to derive the median stellar mass for galaxies at each redshift brighter than $M'_{\mathrm{UV}}(z)$. We present these stellar masses in table 1. Both the scatter in the stellar mass distribution at M'_{UV} and systematics in the stellar mass estimation contribute to the error budget (see e.g., Papovich et al. 2006; Stark et al. 2009; Gonzalez et al. 2010). At $z \lesssim 6$ the scatter in the SFR–stellar mass relation dominates the random errors, and we adopt the scatter $d \log(M^*) = 0.5$ dex (Gonzalez et al. 2010). At $z \gtrsim 6$, random errors from the stellar-population modeling are comparable to the scatter in the SFR–stellar mass relation (Finkelstein et al. 2010; Gonzalez et al. 2010). At $z \sim 7$ and $z \sim 8$ we adopt a scatter of $d \log(M^*) = 0.5$ dex, (Gonzalez et al. 2010). However, at $z = 7$ the 68% the lower bound on the confidence range extends to a factor of order 5 and at $z \sim 8$ it extends to a factor of order 10 (Finkelstein et al. 2010). We adopt these values for the scatter here.

We also derived the stellar mass for galaxies with $n(> M'_*) = 2 \times 10^{-4}$ Mpc^{-3} at $0 < z < 4$ by integrating the stellar mass functions of Marchesini et al. (2009) in the same way as for the luminosity functions above. Table 1 lists these stellar masses, $M'_*(z)$, derived from the mass functions, and converted to a Chabrier IMF. At $z < 3$ the parameters of the stellar mass functions are well constrained for the stellar masses of interest here, and the formal uncertainty on the stellar mass at fixed number density derived by integrating the luminosity function is small, <0.1 dex. At $3 < z < 4$ the stellar mass function is less well constrained, and we find that the uncertainty on the mass function corresponds to uncertainties on the stellar mass at $n(> M^*) = 2 \times 10^{-4}$ Mpc^{-3} of $\log(M'_*/M_\odot) = 10.2^{+0.2}_{-0.7}$. In addition, we adopt a minimum error bar of 0.3 dex (see, e.g., Marchesini et al. 2009) on the stellar masses at fixed number density calculated by integrating the stellar mass functions.

The stellar masses derived at constant number density from the mass functions provide an important comparison sample for the UV-selected galaxies. At $z \lesssim 3$, observations suggest that there exist both infrared luminous and UV-luminous star-forming galaxies (e.g., Papovich et al. 2006), which make a substantial contribution to the cosmic SFR history (e.g., Reddy et al. 2008; Bouwens et al. 2009). There also exist at $z \lesssim 3$ galaxies with suppressed or absent star-formation (e.g., Kriek et al. 2006; van Dokkum et al. 2009; Papovich et al. 2010), although such systems are much rarer or absent at $z \gtrsim 3.5$ (Brammer & van Dokkum 2007; Stutz et al. 2008). The UV luminosity functions at $z \lesssim 3$ may be incomplete for these types of galaxies. The stellar masses at constant number density derived from the Marchesini et al. (2009) mass functions provide a separate measure of the evolution of the stellar mass growth in galaxies selected by means other than the UV luminosity.
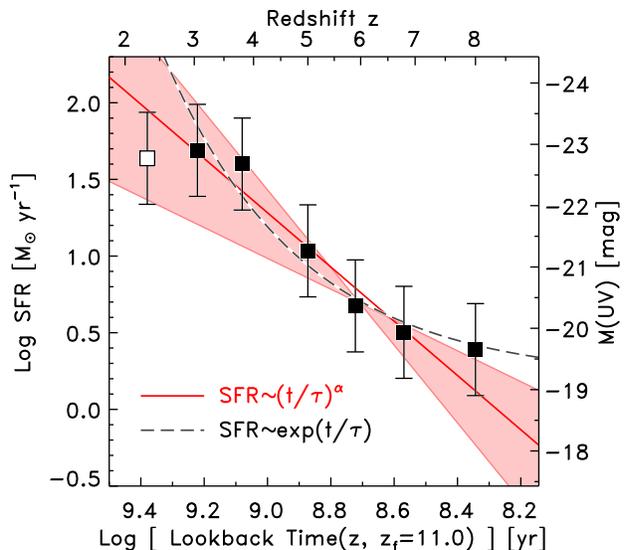

Figure 2. The SFR of galaxies at constant number density $n = 2 \times 10^{-4}$ Mpc^{-3} as a function of lookback time measured from $z = 11$ to the observed redshift, z. The SFRs are derived from the UV luminosity and corrected for dust extinction as discussed in § 2.2. At this number density the SFR increases with time (decreasing redshift) from $z = 8$ to $z = 3$, with data points indicated as filled symbols. The red solid lines and shaded region show fits $\Psi(t) \sim t^\alpha$ to the data from $3 < z < 8$ with parameters and 68% confidence range given in the text. The power-law fit formally has a better goodness-of-fit than the black dashed line, which shows a model where the SFR increases exponentially in time, $\Psi(t) \sim \exp(t/\tau)$. The SFR unambiguously increases smoothly with time from $z = 8$ to $z = 3$. Galaxies at $z < 3$ appear to depart from this evolution, and we indicate the datum at $z = 2.3$ with an open symbol.

3 THE STAR FORMATION HISTORIES OF DISTANT GALAXIES

Figure 2 shows the evolution of the dust-corrected SFR averaged over galaxy populations with $n = 2 \times 10^{-4}$ as a function of lookback time, calculated from a formation redshift $z_f = 11$ to the observed redshift,[3] using the data in table 1. There is an unambiguous smooth increase in the SFR from $z = 8$ to 3. The relationship is consistent with a power law, described by

$$\frac{\Psi(z)}{1 \, M_\odot \, \mathrm{yr}^{-1}} = (t/\tau)^\alpha \tag{3}$$

with $\alpha = 1.7 \pm 0.2$ and $\tau = 180 \pm 40$ Myr fitted over the data from $z = 8$ to 3. We adopt here the power-law fit as it formally has a better goodness-of-fit compared to other simple functions, although it is not a unique representation of the data. Fitting a model to the data where the SFR increases exponentially in time, $\Psi(z) = \Psi_0 \exp(t/\tau)$, gives a minimum $\chi^2 = 1.1$ for 4 degrees of freedom (for $\tau = 420$ Myr and $\Psi_0 = 1.4 \, M_\odot \, \mathrm{yr}^{-1}$), compared to $\chi^2 = 0.66$ for 4 degrees of freedom for the power-law fit above. However, statistically these fits are indistinguishable statistically.

---

[3] The choice of formation redshift $z_f = 11$ is arbitrary and does not affect our conclusions. Changing the formation redshift adds only a constant offset in time to equation 3.

Here, we concentrate on the evolution of galaxy properties at constant number density $n = 2 \times 10^{-4}$ because this describes the evolution of "typical" galaxies (§ 2), and this is where the UV data are most complete (see references in table 1). However, we also studied how the SFH varies with galaxy number density, ranging from $n = 1 \times 10^{-3}$ Mpc^{-3} (corresponding to fainter galaxies with $\sim L^* + 1$ mag) to $n = 4 \times 10^{-5}$ Mpc^{-3} (corresponding to brighter galaxies with $\sim L^* - 0.5$ mag). We observe a modest change in the slope of equation 3 for these samples, from $\alpha = 1.5$ at $n = 1 \times 10^{-3}$ Mpc^{-3} to $\alpha = 1.9$ at $n = 4 \times 10^{-5}$ Mpc^{-3}, but these are consistent within the measured uncertainty, $\delta\alpha = 0.2$. However, the normalization ($\tau^{-\alpha}$) changes relative to that for $n = 2 \times 10^{-4}$ Mpc^{-3} by a factor of $1/22$ at $n = 1 \times 10^{-3}$ Mpc^{-3} to a factor of 12 at $n = 4 \times 10^{-5}$ Mpc^{-3}. Therefore, over the range of number densities considered here ($n = 4 \times 10^{-5} - 1 \times 10^{-3}$ Mpc^{-3}) galaxies experience SFRs that increase as a power-law in time with a slope, α, that is approximately constant. The SFR scales only by a multiplicative factor related to number density (or mass, similar to the simulations of Finlator et al. 2010), where galaxies with higher number density (lower UV luminosity) experience slower evolution (e.g., Bouwens et al. 2010a).

At $z < 3$ the SFRs derived for UV-selected galaxies appear to depart from the SFH in equation 3 (figure 2). At $z \sim 2 - 3$ galaxies with UV luminosities near L^* show a significant heterogeneity in their dust properties, and galaxies at fixed UV luminosity include both intrinsically less luminous galaxies with less dust extinction and intrinsically more luminous galaxies whose UV emission is obscured by dust (Reddy et al. 2010), and so we may expect the departure from the derived SFH. However, our derived SFH is consistent with the space density of K-selected ultraluminous IR galaxies (ULIRGs) at $1.5 < z < 2.5$, which have $n = 2 \times 10^{-4}$ Mpc^{-3} and $\langle \Psi \rangle = 120\ M_\odot$ yr^{-1} (Daddi et al. 2007). Therefore, while UV-selected samples seem incomplete for star-forming galaxies at redshifts $z \lesssim 3$, the derived SFH remains consistent when we include observations of obscured galaxies.

Therefore, galaxies with this constant number density have average SFRs that increase with time for redshifts $3 < z < 8$. This is similar to expectations from theory (e.g., Robertson et al. 2004; De Lucia et al. 2006; Finlator et al. 2006, 2010; Brooks et al. 2009), which predict rising SFHs over this redshift range. We stress that the SFHs we derived here describe the *cosmologically average* evolution of the galaxy population at these redshifts, and individual galaxies likely experience unique SFHs, including stochastic bursts and periods of reduced star-formation. In particular, at later times, $z \lesssim 3$, the SFHs of galaxies seemingly plateau, and at later times galaxies must experience SFHs that decline with time in order to explain the existence of lower redshift galaxies with evolved stellar populations evidenced by the existence of strong 4000 Å/Balmer breaks by $z \sim 2$ (e.g., Kriek et al. 2006). Nevertheless, as we discuss below (§ 4), the *average* smoothly rising SFHs for the galaxy population at early times reproduce the stellar mass growth in galaxies. We therefore, conclude that galaxies with this constant number density experience rising SFHs during the epoch demarcated by $3 < z < 8$.
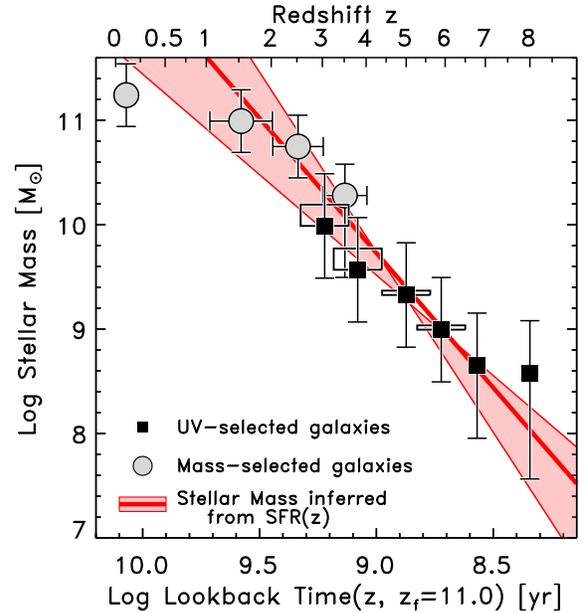

Figure 3. The stellar mass of galaxies as a function of lookback time for galaxies with constant number density. Filled squares show the stellar masses for galaxies with UV luminosities such that $n(< M'_{\rm UV}) = 2 \times 10^{-4}$ Mpc^{-3} from $z = 8$ to 3. The heavy red line and shaded region shows the possible range of stellar mass evolution expected from SFH measured in figure 2. This line is not a fit, as we have made no adjustments to the normalization or slope of this line. The stellar mass growth expected from the measured SFH agrees with the data for UV-selected galaxies at $3 < z < 8$. The measured masses for UV samples at $z < 4$ are slightly below the expected evolution for possible reasons discussed in the text. The filled circles show the evolving stellar masses for galaxies with stellar mass such that $n(> M'_*) = 2 \times 10^{-4}$ Mpc^{-3} (Marchesini et al. 2009). These follow the expected stellar masses from the SFH for redshifts $z \gtrsim 1$. Therefore, the SFH and stellar mass growth are consistent over this redshift range.

4 THE EVOLVING SFR-STELLAR MASS RELATION

The measured SFH provides a direct prediction for the stellar mass evolution for galaxies at this constant number density. For a SFR that evolves as $\Psi(t) \sim t^\alpha$ (equation 3) the stellar mass evolves roughly as $M_*(t) \sim \int \Psi(t)\,dt \sim t^{(\alpha+1)}$. However, one must account for stellar-mass loss due to baryonic gas returned to the ISM of a galaxy from stellar evolution. We therefore computed the expected stellar mass evolution using the SFH from equation 3 with the 2007 version of the Bruzual & Charlot (2003) stellar-synthesis model. We use an input stellar population with $Z = 0.2\ Z_\odot$ metallicity and a Chabrier IMF with no chemical evolution.

Figure 3 shows the evolving stellar mass, M'_*, as a function of lookback time for galaxies with $n = 2 \times 10^{-4}$ Mpc^{-3}. The measured masses of the UV-selected galaxies at this number density are shown as black squares. The heavy red line and shaded region in figure 3 shows the *expected* increase in the stellar mass from the range of SFHs in figure 2. It is important to note that the red curves in figure 3 are not fits to the data, but rather predictions from the derived SFH.

The stellar mass evolution of the UV-selected galaxies at $3 < z < 8$ agree well with this expected growth from the measured SFR history. At $z \sim 8$ the stellar mass for UV-selected galaxies with this number density lie above the expected value, although still within the scatter.

At $z \lesssim 4$ there is slight evidence that stellar masses for the UV samples fall below the expected trend by about 0.3 dex (although again within the scatter). This could be symptomatic of older stellar populations with high mass-to-light ratios which are plausible to the limits of the data (e.g., Papovich et al. 2001; Shapley et al. 2005). Alternatively, the stellar masses derived for the UV samples assumed SFHs that are either constant or decline with time, rather than increase with time. As discussed in Appendix B, stellar masses from rising SFHs are larger by $\approx$0.2 dex for galaxies at $z \sim 3 - 4$ compared to models with SFRs that are constant or decline with time (see also Lee et al. 2010b). In contrast the stellar masses from models with rising SFRs are only <0.1 dex higher at $z \sim 5 - 6$. These shifts are indicated by the open boxes in figure 3, and they would account for most of the observed offset. Furthermore, this offset may be also indicative of the fact that at $z \sim 2 - 3$ galaxies with UV luminosities near L^* show a significant heterogeneity in their dust properties (see § 3, and Reddy et al. 2010), or as a result of the scatter in the UV-luminosity–dark matter relation (see Appendix A). Lastly, by $z \lesssim 3$ there exist massive galaxies with "suppressed" SFRs (e.g., Kriek et al. 2006), which could be missed by the UV selection. These effects may bias the derived stellar masses for these galaxies to lower values. In contrast, these effects are less significant at higher redshifts $z \gtrsim 4$ because there has been less time for them to manifest.

Because of potential biases in the UV-luminosity-selected sample, figure 3 also shows the stellar masses for galaxies at $z < 4$ with constant number density, $n(> M'_*) = 2 \times 10^{-4}$ Mpc^{-3}, derived from the mass functions of Marchesini et al. (2009). The selection based on *stellar mass* mitigates most of the biases for the UV galaxies. Remarkably, the evolution of stellar mass for galaxies at constant number density agrees well with the stellar mass growth expected from the SFH for $z \gtrsim 2$. This supports our conclusion that the cosmologically averaged SFHs of distant galaxies are smoothing rising from $z = 8$ to 3 because this matches both the increased UV luminosities and stellar masses of galaxies with this number density.

The models with rising SFHs contrast assumptions that distant galaxies experience SFRs that are either constant or decreasing with time (e.g., Papovich et al. 2001, 2005, 2006; Shapley et al. 2001; Förster-Schreiber et al. 2004; Shapley et al. 2005; Reddy et al. 2006; Förster-Schreiber et al. 2009; Stark et al. 2009; Finkelstein et al. 2010; Labbé et al. 2010a,b). Several other studies have suggested SFHs that increase with time based on the evolution in the SFR-stellar mass relation at high redshifts ($z \lesssim 6$) (Renzini 2009; Stark et al. 2009; Maraston et al. 2010) and also based on theoretical motivation (Finlator et al. 2007, 2010). Our analysis demonstrates unambiguously that the cosmologically averaged SFRs for typical galaxies increase smoothly with time (decreasing redshift). Individual galaxies likely deviate from this "smoothly" increasing SFRs because they have formation histories that involve stochastic events with discrete changes in the instantaneous SFR (e.g., Baugh et al. 2005; Finlator et al. 2006, 2007; Somerville et al. 2008), and they may experience SFHs that deviate from the average history derived here. The SFHs that we derive here corresponds to a cosmologically averaged evolution that accounts for the observed evolution of the galaxy populations.

The self-consistency between the rising SFHs and the stellar mass growth constrains jointly (degenerately) both the star formation duty cycle and the slope of the high-mass end of the IMF. Observations of clustering measurements and the correlation and scatter of the SFR-stellar mass relation of high–redshift galaxies imply a high star-formation duty cycle (e.g., Daddi et al. 2007; Labbé et al. 2010a; Lee et al. 2010a). If the duty cycle is near unity for galaxies at $3 < z < 8$, then the consistency between the rising SFHs and stellar mass growth here is evidence that the high-mass end of the IMF in these galaxies must have a slope consistent with that of Chabrier (2003) and Salpeter (1955) when averaged over galaxy populations. Otherwise, there would be a larger offset in the SFR-stellar mass relation, which is not evident in the data.

If the star formation duty cycle is lower as suggested by clustering analyses of (predominantly) sub-L^* sources (e.g., Lee et al. 2009, although see Finlator et al. 2010) and by some models of galaxy formation (e.g., Baugh et al. 2005), then our integrated SFH requires an IMF weighted toward higher mass stars in order to match the measured stellar mass growth. For example, a duty cycle of 50% would require a change of ≈ 0.2 to the slope of the IMF to produce a higher ratio of the number of O-type stars to the number of G-type stars compared to that produced by a Salpeter-like IMF. This is similar to the findings of Baldry & Glazebrook (2003) based on SFHs derived from the UV to IR luminosity densities of low-redshift galaxies. Such top-heavy IMFs have been also proposed to explain the joint cosmic evolution of the stellar mass and SFR densities (e.g., Baugh et al. 2005; Davé 2008; Lacey et al. 2008), although these are more extreme IMFs than the change described above. Lastly, our results are unable to constrain the low-mass end of the IMF as any change in the shape of lower mass limit simply scale both the SFR and stellar mass in approximately the same way, shifting both the datapoints and the curve in figure 3 by approximately the same amount.

5 IMPLICATIONS FOR THE GAS MASS AND GAS ACCRETION RATE

The evolution in figures 2 and 3 leads to the conclusion that galaxies increase *both* their SFRs and stellar masses over time. This simply is not possible if galaxies form with a fixed initial cold baryonic gas mass. In this case the SFR would decline with time as the gas mass is converted to stars.

In this section we use our measured evolution in the SFRs and stellar masses of galaxies to predict the evolution of the gas mass in galaxies with with $n = 2 \times 10^{-4}$ Mpc^{-3} at high redshifts. Throughout this section we assume that the local gas-surface density (Σ_{gas}) - SFR surface density (Σ_{SFR}) relation (Schmidt 1959; Kennicutt 1998b) applies to high–redshift galaxies,

$$\frac{\Sigma_{\text{SFR}}}{M_\odot \, \text{yr}^{-1} \text{kpc}^{-2}} = A \left(\frac{\Sigma_{\text{gas}}}{M_\odot \, \text{pc}^{-2}} \right)^N, \qquad (4)$$

where $A = 1.7 \times 10^{-4}$ and $N = 1.4$ have their normal values (though we use the calibration for a Chabrier-like IMF, see Somerville et al. 2008, see also Dutton et al. 2010). The assumption that star–formation in high–redshift galaxies follows this relation remains untested directly at these redshifts, and such tests will require direct measurements of the HI gas, which is currently infeasible. However, recent studies for example by Daddi et al. (2010b) suggest that the star-forming efficiency in normal star-forming disk galaxies is consistent with this assumption, though it may not apply in extreme classes of star-forming galaxies. As the "typical" galaxies studied have SFRs and properties consistent with "normal" star-forming disk galaxies at $z \sim 2$, our assumption is reasonable.

We multiply equation 4 by the areal size of the star-forming region in galaxies, approximated by $a = \pi r_{1/2}^2$, where $r_{1/2}$ is the familiar half-light radius, which relates the gas-mass to the SFR,

$$\frac{\Psi(z)}{1\,M_\odot\,\mathrm{yr}^{-1}} = C \left[\frac{r_{1/2}(z)}{1\,\mathrm{kpc}}\right]^{-0.8} \left[\frac{M_\mathrm{gas}(z)}{10^9\,M_\odot}\right]^{1.4}, \qquad (5)$$

where the constant of proportionality is $C = 1.7$. While the statistical uncertainty on equation 5 is 0.12 dex (Kennicutt 1998b), the true uncertainty may be larger at high redshifts where these relations have not been measured directly.

The rest–frame UV size evolution of high-redshift galaxies has been characterised by Ferguson et al. (2004), who showed that the size evolution for star-forming galaxies from $z \sim 5$ to $z \sim 2$ is consistent with the growth of galaxy disks that scale with the size of their dark matter haloes (Mo et al. 1998), $r(z) \propto H(z)^{-1}$, where $H(z)$ is the Hubble constant at redshift z (consistent with Oesch et al. 2010a). We normalize this relation to produce the characteristic half-light size at $z = 4$ from Ferguson et al., $r(z=4) = 1.7$ kpc with a scatter of approximately 0.6 kpc. The galaxy sizes then evolve as

$$r(z) = 1.7 \left[\frac{H(z)}{H(z=4)}\right]^{-1}\,\mathrm{kpc}, \qquad (6)$$

where $H(z=4) = 430$ km s^{-1} Mpc^{-1}. The extrapolated size evolution from this equation reproduces the sizes measured for $z = 7$ galaxies in *HST*/WFC3 data, $r(z=7) = 0.85$ kpc, consistent with the observations of Oesch et al. (2010a).

Combining equations 5 and 6, and solving for the gas mass yields

$$\frac{M_\mathrm{gas}(z)}{5.9 \times 10^8\,M_\odot} = \left[\frac{\Psi(t)}{1\,M_\odot\,\mathrm{yr}^{-1}}\right]^{5/7} \left[\frac{r(z=4)}{1.7\,\mathrm{kpc}}\right]^{4/7} \qquad (7)$$
$$\times \left[\frac{H(z)}{H(z=4)}\right]^{-4/7}.$$

The uncertainty on the gas mass includes the scatter in the galaxy size measurements, and includes the uncertainty from the SFR-gas mass surface density relationship (a factor of $\delta \log M_\mathrm{gas} = 0.11$ dex). However, as discussed above, equation 7 implicitly assumes the star-formation law from the relation given in equation 4 and neglects any uncertainty on this relation at high redshift.
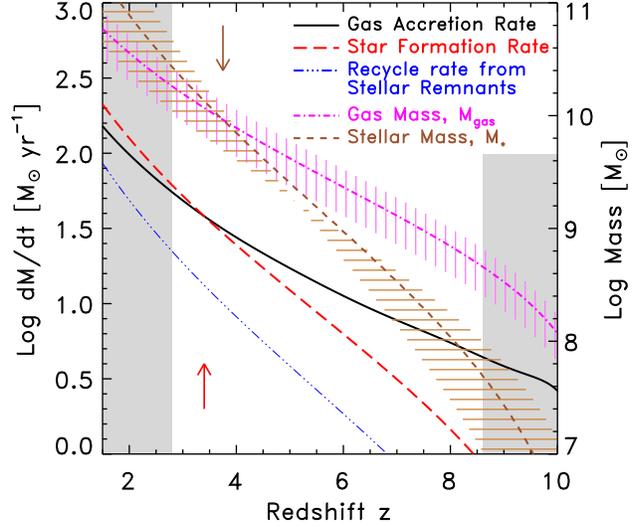

Figure 4. Predicted redshift evolution of the gas accretion rate, $\dot{M}_\mathrm{acc}$ and the gas mass, the derived stellar mass inferred from the empirical SFH, and the empirically derived evolution of the SFR for galaxies with constant number density $n = 2 \times 10^{-4}$ Mpc^{-3}. Here, $\dot{M}_\mathrm{acc}$ is the net gas accretion rate and does not distinguish between the contributions of gas inflow and outflow. The gas mass and gas accretion rate are discussed in the text, and assume the Kennicutt–Schmidt conversion between gas and star-formation surface density. Each curve shows an evolving quantity as indicated in the legend. Gray-shaded regions show redshifts where there is no data, and the curves are extrapolations. The left abscissa shows the scale for the gas accretion rate, the SFR, and the rate of gas mass returned from stellar remnants. The right abscissa shows the scale for gas mass and stellar mass. The downward arrow indicates the redshift where the stellar mass equals the gas mass. The upward arrow indicates the redshift where the SFR equals the gas-mass accretion rate.

5.1 Gas mass and gas accretion rate

Figure 4 shows the derived redshift evolution of the stellar mass (M'_*) inferred from the empirical SFH (§ 4), and the predicted redshift evolution for the gas mass (M'_gas) from equation 7 for galaxies with constant number density $n = 2 \times 10^{-4}$ Mpc^{-3}. The stellar mass increases with time, as discussed in § 4. The gas mass also increases from $z = 8$ to $z = 3$, which is required to fuel the increasing SFRs. Our empirical relations predict that from $z = 10$ to $z = 8$ the gas mass is an order of magnitude larger than the stellar mass for galaxies with $n = 2 \times 10^{-4}$ Mpc^{-3}. The gas mass continues to increase at $z < 8$. While the stellar mass initially lags behind the gas mass, it increases quickly in response to the SFR. Around $z \approx 4$, the stellar mass equals the gas mass for galaxies with this constant number density, and extrapolating to lower redshift the stellar mass becomes the dominant baryonic component for galaxies at this number density.

We use the derivative of the gas mass and the SFR to predict the gas accretion rate, $\dot{M}_\mathrm{acc}$, for these galaxies. The gas accretion rate could be driven by either smooth accretion (e.g., Kereš et al. 2009), or gas delivered via significant mergers (e.g., Robertson & Bullock 2008; Stewart et al. 2008), and differences in these processes do

not affect the simple empirical relations we derive here. Here we do not differentiate between possible physical processes that contribute to the net gas accretion rate but rather we define this to be simply the net rate at which galaxies acquire their baryonic gas. Therefore, the net gas accretion rate here includes the effects of both gas infall and gas outflows (see, e.g., Davé et al. 2006; Dutton et al. 2010). The time-rate-of-change of the gas mass has several components,

$$\dot{M}_{\rm gas}(t) = \dot{M}_{\rm acc}(t) - \Psi(t) + \dot{M}_{\rm rec}(t), \qquad (8)$$

where $\dot{M}_{\rm rec}$ is the amount of gas returned ("recycled") to the galaxy from stellar remnants (taken from the 2007 version of the Bruzual & Charlot 2003 models).

Figure 4 shows the predicted gas accretion rate for galaxies with number density, $n = 2 \times 10^{-4}$ Mpc^{-3} using equation 8 . The figure also shows the SFR and gas-recycling rates. The gas accretion rate increases from $z = 8$ to 3 and keeps pace with or exceeds the measured SFR. At these redshifts these galaxies acquire gas at least as rapidly as it can be converted into stars – this is the "gas accretion epoch" for these galaxies, and is similar to inferences drawn from SPH simulations of galaxy formation (Kereš et al. 2005). At $z \lesssim 4$ the gas-accretion rate declines, and galaxies consume their gas at a rate faster than they acquire it.

Extrapolating the trends in figure 4 to lower redshifts ($z < 3$), our model shows that the stellar mass of galaxies with $n = 2 \times 10^{-4}$ Mpc^{-3} exceeds the available gas mass and the SFR exceeds the gas-accretion rate. These trends can not continue *ad infinitum* as the available gas will eventually be consumed. Indeed, figure 3 indicates that at redshifts $z < 2-3$, the stellar masses of galaxies with $n = 2 \times 10^{-4}$ Mpc^{-3} depart from the expected growth based on the evolving SFR, and this appears consistent with the evolution of neutral gas in absorption-line studies (Prochaska & Wolfe 2009). By $z \sim 2$ some galaxies with the number density considered here have low or suppressed SFRs (Kriek et al. 2006), which presumably have low cold-gas fractions. This implies that the gas accretion rate is decreasing at these redshifts, consistent with galaxy formation simulations (Kereš et al. 2005). Several physical effects and feedback processes have been proposed to prohibit gas cooling and accretion in galaxies (e.g., Birnboim & Dekel 2003; Springel et al. 2005a; Hopkins et al. 2006, 2008; Croton et al. 2006; Somerville et al. 2008), which should apply at the mass scales of galaxies with this number density at these redshifts.

The semi-analytic galaxy formation models of Dutton et al. (2010) find that star-forming galaxies at high redshift have SFRs in a steady state with the total gas mass rate-of-change (gas accretion minus gas losses due to outflows) of $\dot{M}_{\rm gas} \approx \Psi(t)$. The gas accretion rate predicted by our model seems consistent with this conclusion (although large disparities between the gas accretion rate and SFR are not excluded). Dutton et al. (2010) interpret the relative consistency between the SFR and net gas accretion rate as a result of increased gas densities in galaxies. Our empirical results may support this scenario.

5.2 Predictions for galaxy gas-mass fractions

We determine the gas fraction as $f_{\rm gas} = M_{\rm gas}(z) \times [M_{\rm gas}(z) + M_*(z)]^{-1}$ using the evolution of the stellar mass inferred
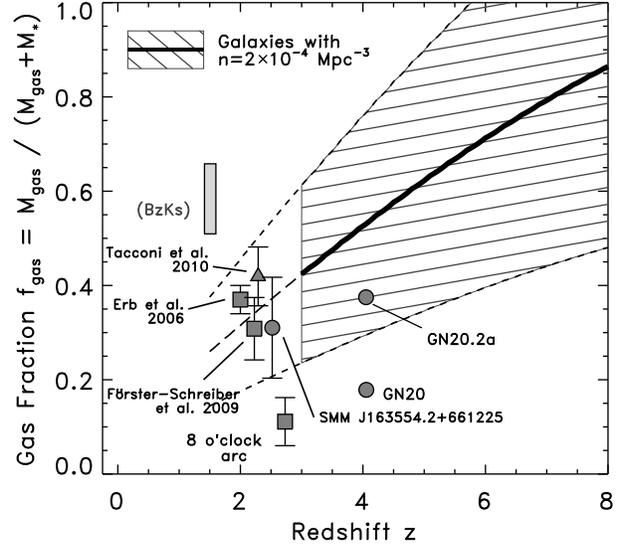

Figure 5. Empirical constraints on the gas fraction, $f_{\rm gas} = M_{\rm gas} \times (M_{\rm gas} + M_*)^{-1}$. The hatched region shows the expected range of average gas fractions for galaxies with constant number density $n = 2 \times 10^{-4}$ for $z = 8$ to $z = 3$. The dashed lines indicate these relations extrapolated to $z = 1.5$. Data points are labelled, and include UV-selected galaxies (filled boxes, Erb et al. 2006; Finkelstein et al. 2009) and sub-mm-selected galaxies (filled circles, Kneib et al. 2005; Papovich et al. 2009; Daddi et al. 2009). The data points for Förster-Schreiber et al. (2009) and Tacconi et al. (2010) show the mean value for galaxies with $z \geqslant 2$ and $M_* > 3 \times 10^{10} M_\odot$, the approximate stellar mass at $z \approx 2-2.5$ such that $n(>M_*') = 2 \times 10^{-4}$ Mpc^{-3}. Our empirical relation generally accounts for the measured gas fractions of these galaxies. There is evidence of mass-dependent evolution. Galaxies with higher stellar masses have lower gas fractions (e.g., the 8 o'clock arc, Finkelstein et al. 2009; GN20, Daddi et al. 2009), implying faster gas-consumption. Likewise, lower mass galaxies have higher gas fractions than what is predicted from the extrapolated relationship for galaxies with $n = 2 \times 10^{-4}$ Mpc^{-3} (Daddi et al. 2010a, see also the lower mass samples of Förster-Schreiber et al. 2009 and Tacconi et al. 2010) .

from the SFH (§ 4) and the evolution of the gas mass from equation 7. The hatched region in figure 5 shows the predicted range of the gas fraction from $z = 8$ to $z = 3$ for galaxies with constant number density $n = 2 \times 10^{-4}$ Mpc^{-3}. The dashed lines show the relation extrapolated to lower redshift. The gas mass fraction for these galaxies decreases with decreasing redshift, parametrised as $f_{\rm gas} \propto (1 + z)^\Gamma$ with $\Gamma \approx 0.9$. This follows from the evolving stellar mass and gas mass derived above. At $z \approx 3-5$ the range of possible gas-mass fractions reach 50%, similar to our conclusions from figure 4.

Figure 5 shows that the predicted gas fractions are consistent with available observations of galaxies at $z \sim 2$ with stellar masses such that $n(> M_*') = 2 \times 10^{-4}$ Mpc^{-3}, including galaxies with gas masses derived from CO measurements Kneib et al. (2005); Daddi et al. (2009); Papovich et al. (2009); Tacconi et al. (2010) and those derived from the SFR surface density inferred from Hα measurements (Erb et al. 2006; Finkelstein et al. 2009; Förster-Schreiber et al. 2009). There is evidence that the

evolution of the gas fractions is mass dependent. Figure 5 also shows gas fractions of several galaxies with masses much greater than the galaxies with $n = 2 \times 10^{-4}$ Mpc^{-3} (these are presumably rarer systems, with lower number density). This includes the gravitationally lensed UV-selected, "8 o'clock arc" at $z = 2.7$ with high stellar mass ($\gtrsim 10^{11}$ $M_\odot$) and low gas fraction, which may have experienced accelerated evolution (Finkelstein et al. 2009). Similarly, the massive sub-mm-selected galaxy GN20 at $z = 4$ has a low gas-mass fraction (Daddi et al. 2009) (see also, Michałowski et al. 2010). These systems show evidence of mergers, enhancing the gas-consumption rate and/or the star-formation efficiency (Daddi et al. 2010b). Because the empirical gas fractions we derive for galaxies with $n = 2 \times 10^{-4}$ Mpc^{-3} agree reasonably with the available observations, galaxies experiencing enhanced gas-consumption rates because of significant mergers seem to be the exception, not the norm at these redshifts.

Galaxies with lower stellar masses than those selected with constant number density, $n = 2 \times 10^{-4}$ Mpc^{-3}, appear to have higher gas-mass fractions (Daddi et al. 2010a, see also the lower mass galaxies in the samples of Förster-Schreiber et al. 2009 and Tacconi et al. 2010). This is further evidence suggesting that the gas-accretion and gas consumption time-scales dependent on galaxy mass.

Our empirical results make very clear predictions for the cosmologically averaged gas masses of galaxies with number density $n = 2 \times 10^{-4}$ Mpc^{-3}, and also that the gas fractions should increase as function of redshift. While the predicted gas masses are consistent with the limited available data, more observations are needed. Future observations from the *Atacama Large Millimeter Array* (ALMA) will have the sensitivity to detect emission from the predicted gas reservoirs in these galaxies, which will test the predictions on the gas masses we make here.

stochastic events and unique SFHs that deviate from the average evolution derived here.

We show that the measured stellar masses for galaxies selected with this constant number density are consistent with the expected stellar mass growth from the derived SFH. If star-forming galaxies at high redshifts have star-formation duty cycles near unity, then this implies that the high-mass end of the stellar initial mass function is approximately Salpeter. For lower duty cycles, our results would require an IMF with high-mass slope weighted toward higher mass stars (by ≈ 0.2 for a duty cycle of $\approx 50\%$). Otherwise, there would be a larger offset in the SFR-stellar mass relation, which is not evident in the data.

We interpret the relation between SFR and stellar mass as a result of net gas accretion (gas outflows combined with gas infall from either smooth accretion or delivered by mergers) coupled with the growth of galaxy disks, where the SFR depends on the local gas-surface density relation. This leads to predictions for the galaxy gas masses and gas accretion rates on galaxies $z = 8$ to $z = 3$. The gas fraction evolves at a rate of $f_{\rm gas} \propto (1+z)^{\Gamma}$, with $\Gamma \approx 0.9$, and we show these gas fractions are in reasonable agreement with available data at $z \sim 2$. These relations imply that at $z > 4$ galaxies selected at this constant number density acquire baryonic gas at least as fast as it can be converted into stars. This is the "gas accretion epoch" for these galaxies. Interpreting this in the context of a semi-analytic model (Dutton et al. 2010) this suggests that the smoothly rising SFHs are a consequence of increased gas densities in these galaxies. At $z < 4$ the SFR in these galaxies overtakes the gas-accretion rate, indicating a period where these galaxies consume gas faster than it is acquired. At redshifts $z \lesssim 3$, galaxies depart from these relations implying that gas accretion is slowed or prevented at later times.

6 SUMMARY

We use observed relations of the SFRs and stellar masses for galaxies to constrain empirically the SFHs of galaxies at $3 < z < 8$. We compare the evolution of galaxies at these redshifts at constant comoving number density, $n(< M'_{\rm UV}) = 2 \times 10^{-4}$ Mpc^{-3}. We show that this allows us to track the evolution of stellar mass and star formation in the direct predecessors and descendants of these galaxies in a relatively meaningful way that is not possible using samples selected either at constant luminosity or constant mass. We summarize our findings as the following.

The galaxies experience cosmologically averaged SFHs with SFRs that grow with time (decreasing redshift) at a rate best described by $\Psi(t) \sim t^{\alpha}$ with $\alpha = 1.7 \pm 0.2$. This excludes model SFHs where the SFR is either constant or declines exponentially in time. We find evidence that galaxies over a range of number density from $n = 4 \times 10^{-5}$ Mpc^{-3} to 1×10^{-3} Mpc^{-3} (corresponding to galaxies with luminosities $< L^*_{\rm UV} - 0.5$ mag and $< L^*_{\rm UV} + 1$ mag, respectively), experience SFHs with similar power-law increases with time, but differ by a multiplicative scale factor. These results are similar to expectations from theory (e.g., Finlator et al. 2010). We reemphasize that these SFHs correspond to the cosmologically averaged evolution of the galaxy populations with these number densities. Individual galaxies experience

REFERENCES

Adelberger K. L., Steidel C. C., Pettini M., Shapley A. E., Reddy N. A., Erb D. K., 2005, ApJ, 619, 697

Baldry I. K., Glazebrook K., 2003, ApJ, 593, 258

Balestra I., et al., 2010, A&A, 512, 12

Baugh C. M., Lacey C. G., Frenk C. S., Granato G. L., Silva L., Bressan A., Benson A. J., Cole S., 2005, MNRAS, 356, 1191

Bertone S., De Lucia G., Thomas P. A., 2007, MNRAS, 379, 1143

Birnboim Y., Dekel A., 2003, MNRAS, 345, 349

Bouché N., et al., 2010, ApJ, 718, 1001

Bournaud F., et al., 2008, A&A, 486, 741

Bouwens R. J., Illingworth G. D., Blakeslee J. P., Franx M., 2006, ApJ, 653, 53

Bouwens R. J., et al., 2009, ApJ, 705, 936

Bouwens R. J., Illingworth G. D., Franx M., Ford H., 2007, ApJ, 670, 928

Bouwens R. J., et al., 2010a, ApJ, submitted, arXiv:1006.4360

Bouwens R. J., et al., 2010b, ApJ, 709, L133

Bouwens R. J., Illingworth G. D., Oesch P. A., Trenti M., Stiavelli M., Carollo C. M., Franx M., van Dokkum P. G., Labbé I., Magee D., 2010c, ApJ, 708, L69

Bouwens R. J., et al., 2004, ApJ, 606, L25

Brammer G. B., van Dokkum P. G., 2007, ApJ, 654, L107

Brooks A. M., Governato F., Quinn T., Brook C. B., Wadsley J., 2009, ApJ, 694, 396

Bruzual G., Charlot S., 2003, MNRAS, 344, 1000

Calzetti D., Armus L., Bohlin R. C., Kinney A. L., Koornneef J., Storchi-Bergmann T., 2000, ApJ, 533, 682

Carilli C. L., et al., 2010, ApJ, 714, 1407

Chabrier G., 2003, PASP, 115, 763

Conroy C., Wechsler R. H., 2009, ApJ, 696, 620

Cristiani S., et al., 2000, A&A, 359, 489

Croton D. J., et al., 2006, MNRAS, 365, 11

Daddi E., et al., 2010a, ApJ, 713, 686

Daddi E., et al., 2009, ApJ, 694, 1517

Daddi E., et al., 2007, ApJ, 670, 156

Daddi E., et al., 2010b, ApJ, 714, L118

Davé R., 2008, MNRAS, 385, 147

Davé R., Finlator K., Oppenheimer B. D., 2006, MNRAS, 370, 273

De Lucia G., Springel V., White S. D. M., Croton D., Kauffmann G., 2006, MNRAS, 366, 499

Dekel A., Sari R., Ceverino D., 2009, ApJ, 703, 785

Dutton A. A., van den Bosch F. C., Dekel A., 2010, MNRAS, 608

Elmegreen B. G., Bournaud F., Elmegreen D. M., 2008, ApJ, 688, 67

Erb D. K., 2008, ApJ, 674, 151

Erb D. K., Steidel C. C., Shapley A. E., Pettini M., Reddy N. A., Adelberger K. L., 2006, ApJ, 646, 107

Ferguson H. C., et al., 2004, ApJ, 600, L107

Finkelstein S. L., Papovich C., Giavalisco M., Reddy N. A., Ferguson H. C., Koekemoer A. M., Dickinson M., 2010, ApJ, 719, 1250

Finkelstein S. L., Papovich C., Rudnick G., Egami E., Le Floc'h E., Rieke M. J., Rigby J. R., Willmer C. N. A., 2009, ApJ, 700, 376

Finlator K., Davé R., Oppenheimer B. D., 2007, MNRAS, 376, 1861

Finlator K., Davé R., Papovich C., Hernquist L., 2006, ApJ, 639, 672

Finlator K., Oppenheimer B. D., Davé R., 2010, MNRAS, submitted, arXiv:1005.4066

Förster-Schreiber N. M., et al., 2009, ApJ, 706, 1364

Förster-Schreiber N. M., et al., 2004, ApJ, 616, 40

Genzel R., et al., 2008, ApJ, 687, 59

Giavalisco M., Dickinson M., 2001, ApJ, 550, 177

Gonzalez V., Labbe I., Bouwens R., Illingworth G., Franx M., Kriek M., 2010, ApJ, submitted, arXiv:1008.3901

Guo Q., White S. D. M., 2008, MNRAS, 384, 2

Hopkins P. F., Cox T. J., Kereš D., Hernquist L., 2008, ApJS, 175, 390

Hopkins P. F., Hernquist L., Cox T. J., Di Matteo T., Robertson B., Springel V., 2006, ApJS, 163, 1

Kennicutt Jr. R. C., 1998a, ARA&A, 36, 189

—, 1998b, ApJ, 498, 541

Kereš D., Katz N., Fardal M., Davé R., Weinberg D. H., 2009, MNRAS, 395, 160

Kereš D., Katz N., Weinberg D. H., Davé R., 2005, MNRAS, 363, 2

Kneib J., Neri R., Smail I., Blain A., Sheth K., van der Werf P., Knudsen K. K., 2005, A&A, 434, 819

Kriek M., et al., 2006, ApJ, 649, L71

Kroupa P., 2001, MNRAS, 322, 231

Labbé I., et al., 2010a, ApJ, 716, L103

Labbé I., et al., 2010b, ApJ, 708, L26

Lacey C. G., Baugh C. M., Frenk C. S., Silva L., Granato G. L., Bressan A., 2008, MNRAS, 385, 1155

Laidler V. G., et al., 2007, PASP, 119, 1325

Law D. R., Steidel C. C., Erb D. K., Larkin J. E., Pettini M., Shapley A. E., Wright S. A., 2009, ApJ, 697, 2057

Lee K., et al., 2010a, ApJ, submitted, arXiv:1009.3022

Lee K., Giavalisco M., Conroy C., Wechsler R. H., Ferguson H. C., Somerville R. S., Dickinson M. E., Urry C. M., 2009, ApJ, 695, 368

Lee K., Giavalisco M., Gnedin O. Y., Somerville R. S., Ferguson H. C., Dickinson M., Ouchi M., 2006, ApJ, 642, 63

Lee S., Ferguson H. C., Somerville R. S., Wiklind T., Giavalisco M., 2010b, ApJ, submitted, arXiv:1010.1966

Magdis G. E., Rigopoulou D., Huang J., Fazio G. G., 2010, MNRAS, 401, 1521

Maraston C., Pforr J., Renzini A., Daddi E., Dickinson M., Cimatti A., Tonini C., 2010, MNRAS, 407, 830

Marchesini D., van Dokkum P. G., Förster Schreiber N. M., Franx M., Labbé I., Wuyts S., 2009, ApJ, 701, 1765

McLure R. J., Dunlop J. S., Cirasuolo M., Koekemoer A. M., Sabbi E., Stark D. P., Targett T. A., Ellis R. S., 2010, MNRAS, 126

Michałowski M. J., Watson D., Hjorth J., 2010, ApJ, 712, 942

Mo H. J., Mao S., White S. D. M., 1998, MNRAS, 295, 319

Naab T., Johansson P. H., Ostriker J. P., Efstathiou G., 2007, ApJ, 658, 710

Noeske K. G., et al., 2007, ApJ, 660, L43

Oesch P. A., et al., 2010a, ApJ, 709, L21

Oesch P. A., et al., 2010b, ApJ, 709, L16

Oke J. B., Gunn J. E., 1983, ApJ, 266, 713

Papovich C., Dickinson M., Ferguson H. C., 2001, ApJ, 559, 620

Papovich C., Dickinson M., Giavalisco M., Conselice C. J., Ferguson H. C., 2005, ApJ, 631, 101

Papovich C., Rudnick G., Rigby J. R., Willmer C. N. A.,

Smith J., Finkelstein S. L., Egami E., Rieke M., 2009, ApJ, 704, 1506

Papovich C., et al., 2006, ApJ, 640, 92

Papovich C., et al., 2010, ApJ, 716, 1503

Popesso P., et al., 2009, A&A, 494, 443

Prochaska J. X., Wolfe A. M., 2009, ApJ, 696, 1543

Reddy N. A., Erb D. K., Pettini M., Steidel C. C., Shapley A. E., 2010, ApJ, 712, 1070

Reddy N. A., Steidel C. C., 2009, ApJ, 692, 778

Reddy N. A., Steidel C. C., Erb D. K., Shapley A. E., Pettini M., 2006, ApJ, 653, 1004

Reddy N. A., Steidel C. C., Pettini M., Adelberger K. L., Shapley A. E., Erb D. K., Dickinson M., 2008, ApJS, 175, 48

Renzini A., 2009, MNRAS, 398, L58

Robertson B., Yoshida N., Springel V., Hernquist L., 2004, ApJ, 606, 32

Robertson B. E., Bullock J. S., 2008, ApJ, 685, L27

Salpeter E. E., 1955, ApJ, 121, 161

Schmidt M., 1959, ApJ, 129, 243

Shapley A. E., Steidel C. C., Adelberger K. L., Dickinson M., Giavalisco M., Pettini M., 2001, ApJ, 562, 95

Shapley A. E., Steidel C. C., Erb D. K., Reddy N. A., Adelberger K. L., Pettini M., Barmby P., Huang J., 2005, ApJ, 626, 698

Somerville R. S., Hopkins P. F., Cox T. J., Robertson B. E., Hernquist L., 2008, MNRAS, 391, 481

Somerville R. S., Primack J. R., Faber S. M., 2001, MNRAS, 320, 504

Springel V., Di Matteo T., Hernquist L., 2005a, ApJ, 620, L79

Springel V., White S. D. M., Jenkins A., Frenk C. S., Yoshida N., Gao L., Navarro J., Thacker R., Croton D., Helly J., Peacock J. A., Cole S., Thomas P., Couchman H., Evrard A., Colberg J., Pearce F., 2005b, Nature, 435, 629

Stanway E. R., et al., 2004, ApJ, 604, L13

Stark D. P., Ellis R. S., Bunker A., Bundy K., Targett T., Benson A., Lacy M., 2009, ApJ, 697, 1493

Stewart K. R., Bullock J. S., Wechsler R. H., Maller A. H., Zentner A. R., 2008, ApJ, 683, 597

Stutz A. M., Papovich C., Eisenstein D. J., 2008, ApJ, 677, 828

Tacconi L. J., et al., 2010, Nature, 463, 781

van Dokkum P. G., Kriek M., Franx M., 2009, Nature, 460, 717

van Dokkum P. G., et al., 2010, ApJ, 709, 1018

Vanzella E., et al., 2008, A&A, 478, 83

Wright S. A., Larkin J. E., Law D. R., Steidel C. C., Shapley A. E., Erb D. K., 2009, ApJ, 699, 421

APPENDIX A: ON GALAXIES AT CONSTANT NUMBER DENSITY

In this paper we have studied the evolution of galaxies from $3 < z < 8$ at fixed number density. This has the advantage that in principle it traces the evolution of the progenitors and descendants of galaxies as a function of redshift in a way that is not possible using other methods such as selection at constant luminosity or mass, quantities which themselves evolve with time. It is also relatively straightforward
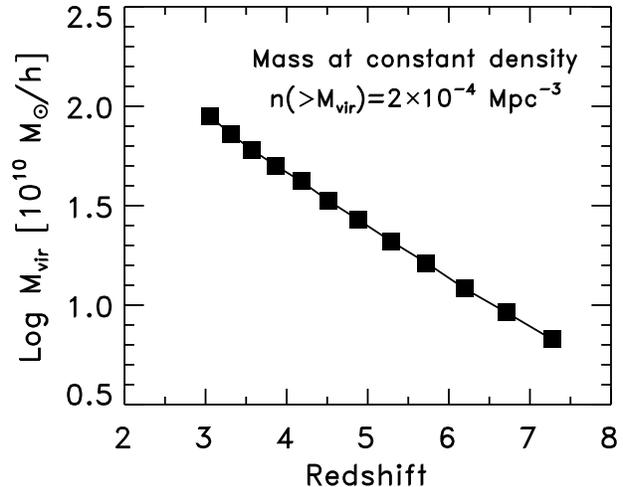

Figure A1. The evolution of halo mass at constant number density from the Millennium simulation (Springel et al. 2005b). The datapoints show the halo mass, $M_{\rm vir}$, corresponding to constant number density, $n(> M_{\rm vir}) = 2 \times 10^{-4}$ Mpc^{-3}, at each redshift. Halos selected at constant number density grow in mass by roughly a factor of 10, similar to the growth in stellar mass for galaxies we observe at these redshifts (figure 3).

to compare results from observational galaxy surveys to expectations from theory. van Dokkum et al. (2010) applied a similar selection to study the size evolution of massive galaxies at $z \lesssim 2$. They quantified the effects of mergers on their selection using Monte Carlo simulations of the mass function, and concluded that selection at constant number density produces homogeneous samples at different redshifts with low contamination unless haloes grow only via one-to-one mergers. Based on theoretical arguements they argued that evolution driven by major mergers is highly unlikely (e.g., Naab et al. 2007; Guo & White 2008).

We studied how well selecting galaxies at constant number density tracks the descendants and progenitors of galaxies at different redshifts by exploring the halo-merger trees and mass functions from the Millennium simulation (e.g., Springel et al. 2005b). This allows us to study halo growth via mergers and accretion in a physically motivated simulation that reproduces observational clustering statistics. We selected dark-matter haloes with mass, $M_{\rm vir}$, such that $n(> M_{\rm vir}, z) = 2 \times 10^{-4}$ Mpc^{-3}, for redshifts $3 < z < 7.3$. Figure A1 shows that the mass corresponding to this constant number density increases by more than an order of magnitude over this redshift range (similar to the growth in stellar mass in galaxies we observe in figure 3).

We tracked the descendants of the halos selected in the Millennium simulation that have halo mass such that $n(> M_{\rm vir}, z) = 2 \times 10^{-4}$ Mpc^{-3} at $z < 7.3$ and have a progenitor at $z = 7.3$ with mass $M_{\rm vir}$ such that it has the same number density. The top panel of figure A2 shows the "completeness" fraction, which is defined as the ratio of the number of the descendants of the galaxies that reside in haloes with mass that satisfies $n(> M_{\rm vir}) = 2 \times 10^{-4}$ Mpc^{-3} at lower redshift z compared to the number at $z = 7.3$. The completeness fraction is related to the "contamination" fraction, which is the fraction of those haloes at red-
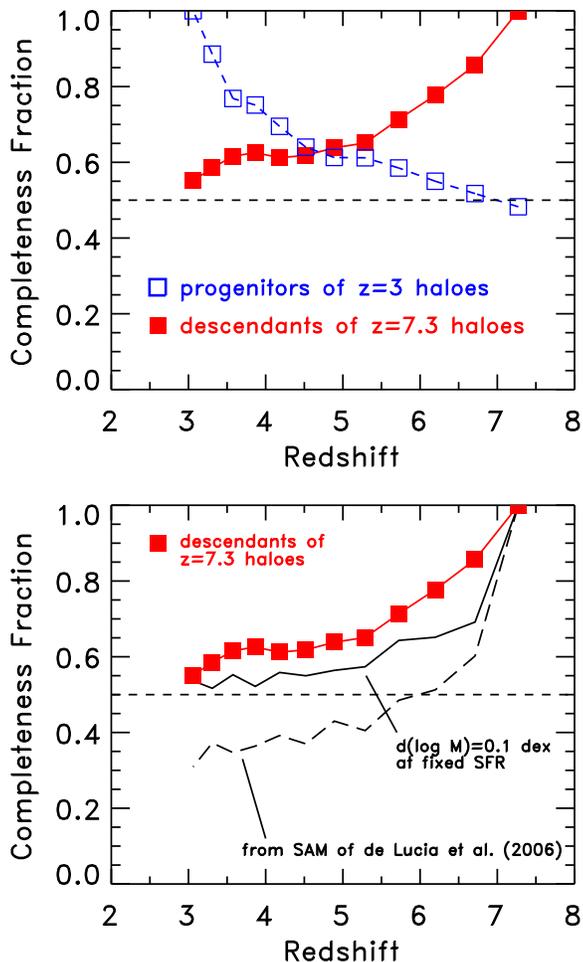
Figure A2. The top panel shows the completeness of the descendants and progenitors of dark matter halos at different redshifts. The filled squares show the descendant completeness, defined as the fraction of haloes selected at redshift z with mass such that $n(>M_{\rm vir}) = 2 \times 10^{-4}$ Mpc^{-3} and a progenitor at $z = 7.3$ selected at this number density. The open squares and dashed curve shows the completeness for the progenitors of haloes selected at constant number density at $z = 3$. The bottom panel shows how the completeness changes for galaxies selected at fixed SFR with $n(>\Psi) = 2 \times 10^{-4}$ Mpc^{-3}. The filled squares show the completeness for the halos as in the top panel. The dashed curve shows the completeness for the SAM of De Lucia et al. (2006) using the Millennium simulation. The solid curve shows the completeness assuming that the scatter in halo mass is $d(\log M_{\rm vir}) = 0.1$ dex at fixed SFR, as predicted by the models of Dutton et al. (2010) and Finlator et al. (2010).

shift z with mass such that $n(>M_{\rm vir}) = 2 \times 10^{-4}$ Mpc^{-3} but lacking a progenitor with mass such that $n(>M_{\rm vir}) = 2 \times 10^{-4}$ Mpc^{-3} at $z = 7.3$. Because the number density is constant, the completeness and contamination are related by $(1 - \text{completeness}) = \text{contamination}$.

The completeness fraction drops from unity at $z \approx 7.3$ to approximately 0.6–0.7 for $3 < z < 6$. This implies that selecting halos at this number density identifies the majority of the lower-redshift descendants of objects selected at higher redshift. The haloes whose descendants are "missing" have masses < 0.5 dex below the mass limit for this number density. Arguably if we allowed an evolving number density criterion, then we would select more of the halo descendants, increasing the completeness fraction. However, this would come at the cost of increasing the contamination fraction. Similarly, the haloes that *contaminate* the sample have masses at $z = 7.3$ within < 0.5 dex of the mass limit for the number density selection. Because these contaminants have masses close to the selection threshold, we expect they will have similar evolutionary paths and SFHs as the galaxies selected at constant number density (see § 3 and discussion in Finlator et al. 2010).

Figure A2 also shows the completeness of the *progenitors* of haloes selected at $z = 3$ with $n(>M_{\rm vir}) = 2 \times 10^{-4}$ Mpc^{-3}. The conclusions are similar as those for the descendants of the $z = 7.3$ haloes. The progenitor completeness becomes lower at higher redshifts compared to the descendant completeness, as the progenitors of $z = 3$ haloes become slightly less massive than the required value for the number density selection. We conclude that selecting halos at constant number density traces the majority of the descendants and progenitors of galaxy halos at $3 < z < 7.3$, and therefore provide samples to study the direct evolution in these populations.

However, thus far we have discussed the completeness in the descendants and progenitors of only the dark matter haloes. To make the connection to observed galaxies, we make the *ansatz* that there is zero scatter between galaxy mass, galaxy luminosity, and halo mass,

$$n_{\rm gal}(>L_{\rm UV}) = n_{\rm gal}(>M^*) = n_{\rm halo}(>M_{\rm vir}). \quad (A1)$$

The true scatter in equation A1 is very poorly known theoretically, with values ranging from $d(\log M_{\rm vir}) = 0.05 - 0.1$ dex at fixed SFR (e.g., Dutton et al. 2010; Finlator et al. 2010) to 0.3 dex (e.g., De Lucia et al. 2006; Bertone et al. 2007). Our assumption of zero scatter is the simplest assumption possible. It allows us to study the evolution of galaxies at constant number density without reliance on theoretical expectations, and it allows the straightforward comparison to theoretical predictions for simulated galaxies selected in the same way. Moreover, this assumption is justified by observations that find a tight relationship between UV luminosity and halo mass (e.g., Giavalisco & Dickinson 2001; Adelberger et al. 2005; Lee et al. 2006, 2009). Even if there is appreciable scatter, we find evidence that the SFHs of galaxies may vary only by a scale factor (see § 3), consistent with expectations from simulations (e.g., Finlator et al. 2010). Therefore, even if our assumption of zero scatter between UV luminosity and dark-matter halo mass is simplistic, the derived SFHs still should be reasonably accurate.

Nevertheless, a non-zero scatter between UV luminosity and dark matter halo mass would affect the completeness in the descendants and progenitors of galaxies selected at constant number density at different redshifts. We study this effect using several models of galaxy evolution. For the De Lucia et al. (2006) SAM models we select galaxies at $z = 7.3$ with SFR such that $n(>\Psi) = 2 \times 10^{-4}$ Mpc^{-3} and track the descendants within the Millennium merger-tree at lower redshift directly. Because these models have the highest scatter at fixed SFR, $d \log M_{\rm vir} = 0.3$ dex, the completeness in the descendants selected with constant number density at lower redshift declines. The bottom panel of fig-

ure A2 shows that the completeness drops to 40% in these cases. However, we consider this model to be extreme as it has not been shown to reproduce the UV luminosity functions at high redshift. In contrast, the Dutton et al. (2010) SAMs and Finlator et al. (2010) simulations have lower scatter, $d(\log M_{\rm vir}) = 0.1$ dex, and these models broadly reproduce trends in the SFR-mass and UV luminosity functions at high redshift. For these models we randomly adjust the mass of the dark matter halos in the Millennium simulation by the scatter and reevaluate the completeness. Figure A2 shows that for these models the completeness in the descendants of $z = 7.3$ galaxies remains $>50\%$ for all redshifts $z \geqslant 3$. In this case selection at constant number density selects the majority of the descendants as a function of redshift and has a negligible impact on our conclusions.

Therefore, even if there is appreciable scatter in the SFR-halo mass relation, selection at constant number density still tracks the descendants of the higher-redshift galaxies, albeit with a higher contamination fraction. Furthermore, we find that the majority of the the descendants that are "missed" by this selection as well as those galaxies that "contaminate" this selection (those without a progenitor selected at higher redshift) have SFRs within a factor of 3 compared to the limit for constant number density. These galaxies appear to have evolutionary histories similar to the galaxies selected at constant number density and scatter into and out of the sample at each redshift. While this reduces the ability of the selection technique to track the direct progenitors and descendants of the galaxy population, it should introduce only a weak affect on the derived SFH.

We therefore conclude that selection at constant number density provides relatively fair, homogeneous samples with which to study galaxy descendants and progenitors. The conclusions here are similar to those of van Dokkum et al. (2010) (see discussion at the beginning of this section). Comparing galaxy samples at constant number density seems preferable to study galaxy SFHs, compared to studies that use luminosity- or mass-selected galaxies. This is for the reason that the latter quantities evolve strongly in time. Samples selected at constant luminosity or stellar mass will be heterogeneous at different redshifts, potentially obfuscating any evolution in these quantities themselves.

APPENDIX B: ON THE STELLAR MASSES DERIVED FROM MODELS WITH RISING SFRS

One of the main conclusions from this study is that the SFRs of galaxies at constant number density increase from $z = 8$ to $z = 3$ and that this SFH is consistent with the evolution of stellar mass in these galaxies. However, their is a potential inconsistency with this later arguement as galaxy stellar masses used to make this comparison were derived from models using either constant or declining SFRs (see § 2.3). Maraston et al. (2010) concluded recently that models with rising SFRs provide better fits to the measured photometry for $z \sim 2$ star-forming galaxies, and produce stellar masses larger than constant or decaying τ models by factors of $\sim 2 - 3$ (see also Lee et al. 2010b). Therefore, it is prudent to consider how the stellar masses of galaxies are affected using models with rising SFRs compared to those for constant or declining SFRs.

We compiled multiwavelength photometry for galaxies in the GOODS-S field with high fidelity spectroscopic redshifts $3.0 < z < 6.0$ (Cristiani et al. 2000; Stanway et al. 2004; Vanzella et al. 2008; Popesso et al. 2009; Balestra et al. 2010). The multiwavelength photometry was originally selected using the ACS z_{850}-band, and includes aperture matched colours in bandpasses from ACS $B_{435}V_{606}i_{775}z_{850}$, ISAAC JHK, and IRAC at 3.6, 4.5, 5.8, and 8.0 μm. The ISAAC and IRAC photometry are measured using TFIT (Laidler et al. 2007) using the ACS z_{850} data as a prior for source positions.

We derived stellar masses for this subsample of GOODS-S galaxies using decaying τ models, $\Psi \sim \exp(-t/\tau)$, following Papovich et al. (2001). We used the 2007 version of the Bruzual & Charlot (2003) models with Chabrier IMF and fixed metallicity of 0.2 $Z_\odot$. We allowed the stellar population age to vary from $10^7 - 2 \times 10^{10}$ yr, with τ in the range $10^6 - 10^{10}$ and $\tau = \infty$ (equivalent to a constant SFR), with dust attenuation following Calzetti et al. (2000) ranging from $A(V) = 0.0 - 2.8$ mag. We then derived stellar masses using the same models, but where the SFRs rise with time following equation 3, and where we fix the age (t) to be the lookback time from the galaxy redshift z to the fiducial formation redshift $z_f = 11$. We allow for the same range of dust attenuation, and we allow the overall normalization of the model to vary in order to fit each galaxy because the evidence suggests that the SFHs of galaxies differ only by a factor that scales with mass (see § 3, and Finlator et al. 2010). We note that this SFH is the cosmological average of galaxies selected at constant number density. In reality individual galaxies will have unique SFHs that likely depart from this model. The point here is not to obtain necessarily the best representative fit to the photometry of each galaxy, but rather to understand how models with rising SFRs affect the derived stellar masses.

Figure B1 shows several examples of galaxies with stellar masses that would fall in a sample selected at constant number density, $n = 2 \times 10^{-4}$ Mpc^{-3}. The curves in each panel show the rising SFH and declining SFH models with the "best-fit" parameter values from the model with the minimum reduced χ^2 value with parameters listed. In all cases the stellar population ages and stellar masses have larger values for models with rising SFHs. The minimum reduced χ^2 are close in all cases. This is a result of the fact that the SFH is poorly constrained by modeling the broad-band photometry of galaxies (e.g., Papovich et al. 2001). However, in general the models with rising SFHs provide fits that are statistically indistinguishable as models with declining models, which is noteworthy given that here we have tested only a single rising SFH (with $\Psi(t) \sim t^{1.7}$) compared to the declining models, which spanned the full range of $e-$ folding time-scales (see above). Finally, we remind the reader that we expect models with rising SFHs to represent *average* galaxies with ongoing star-formation. Realistically, galaxies have individual, stochastic SFHs. In particular, at lower redshifts, $z \lesssim 3$, galaxies will exhibit "suppressed" SFRs, and these are consistent with declining SFHs. The rising SFHs advocated here corresponds to the average evolution of the star-forming galaxy population at early times ($3 \lesssim z \lesssim 8$).

The results of our fitting analysis show that stellar masses derived with rising SFRs generally produce higher stellar masses than decaying τ models, and that the increase
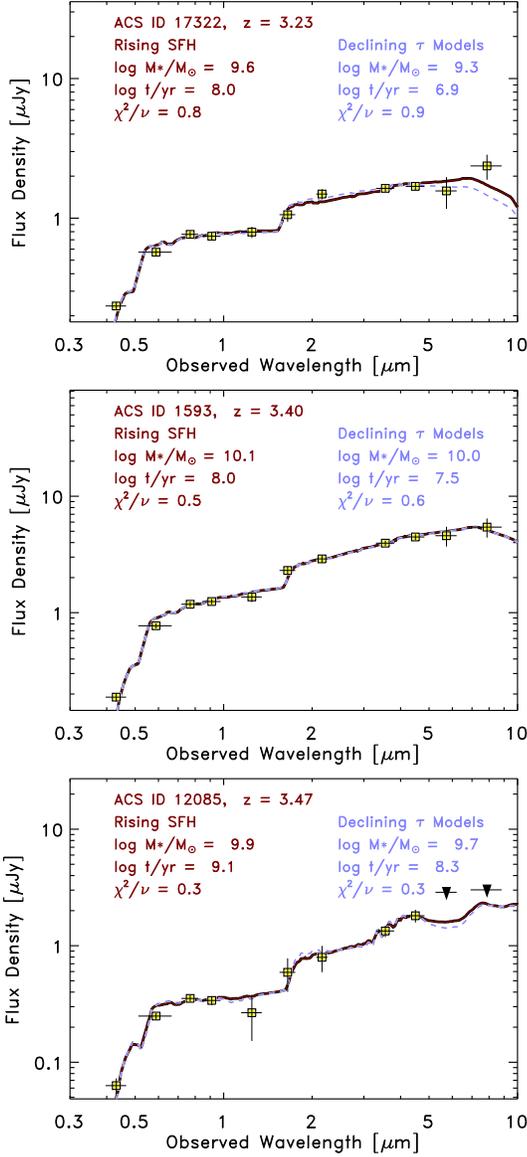
Figure B1. Fits to the broad–band photometry for several galaxies from the spectroscopic GOODS-S subsample. Each panel shows the results for an individual galaxy. The ACS, ISAAC, and IRAC photometry are indicated by yellow squares. The curves show the best-fit models for models with rising SFHs (brownish-red curves) and declining SFHs (light-blue curves) with best-fit parameters inset in each panel. The full range of model parameters used are listed in the text. In general, models with rising SFHs yield higher stellar masses and older ages, but both models have best-fit reduced χ^2 that are statistically generally indistinguishable.

in the stellar masses generally increases with the passage of time. Figure B2 compares the stellar masses derived from the decaying τ models to those derived using the rising SFRs, divided into two subsamples of redshift, $3.0 < z < 4.5$ and $4.5 < z < 6.0$. The stellar masses derived from rising SFHs for galaxies at $3 < z < 4.5$ are a factor of 1.6 higher on average, while the offset is smaller (a factor of 1.1) for galaxies at $4.5 < z < 6.0$. Therefore, if the model SFH posited in § 3 is correct, then the stellar masses of star-forming galax-
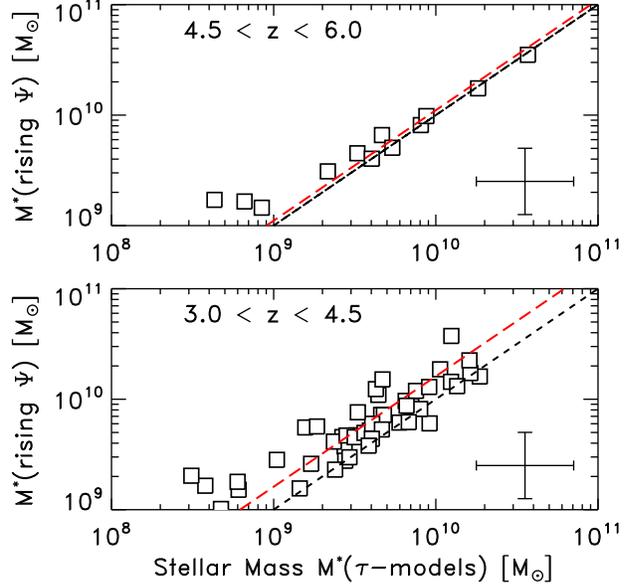

Figure B2. Stellar masses derived from decaying τ models where $\Psi \sim \exp(-t/\tau)$ versus those derived using the rising SFH derived here (equation 3). The panels show galaxies with spectroscopic redshifts from GOODS-S in two redshift bins of $3 < z < 4.5$ and $4.5 < z < 6$. Representative error bars are shown. The black, short-dashed lines show the unity relations. Stellar masses derived with rising SFHs generally produce higher stellar masses than decaying τ models. The increase in stellar mass generally increases with time. The stellar masses derived from models with rising SFRs for galaxies at $3 < z < 4.5$ are a factor of 1.6 higher (indicated by the red, long-dashed line, bottom panel), while the offset is smaller (factor of 1.1, red long-dashed line, top panel) for galaxies at $4.5 < z < 6.0$.

ies at $z \sim 3 - 4$ may need to be revised upwards by factor of order 2, similar to the conclusions of Maraston et al. (2010) (although see Lee et al. 2010b, who find that rising SFHs overpredict stellar masses of galaxies in simulations by factors of up to ~2). The masses of galaxies at $z \gtrsim 4$ are mostly unchanged. Moreover, this increase in stellar mass from rising star-formation histories for galaxies at $z \lesssim 4$ is approximately the amount needed to reconcile the offset between the measured SFRs and stellar masses (figure 3). If the stellar masses of the UV-selected galaxies are higher by 0.2-0.3 dex, it would adjust them closer to the derived SFH.

This paper has been typeset from a TEX/ LATEX file prepared by the author.